Research Article

Effects of single-walled carbon nanotubes and steel fiber on recycled ferrochrome filled electrical conductive mortars

Heydar DEHGHANPOUR[*,1] [iD], **Fatih DOĞAN**[2] [iD], **Serkan SUBAŞI**[3] [iD], **Muhammed MARAŞLI**[3] [iD]

¹Fibrobeton Company, R&D Center, Düzce, Türkiye
²Munzur University, Rare Earth Elements Application and Research Center, Tunceli, Türkiye
³Department of Civil Engineering, Düzce University Faculty of Engineering, Düzce, Türkiye

ABSTRACT

The production of electrically conductive concrete was introduced years ago among construction materials, generally for anti-icing. The present study investigates the electrical, mechanical, dynamic, and microstructural properties of recycled ferrochrome filled cementitious mortars containing single-walled carbon nanotubes (SWCNTs) and steel fiber. Within the scope of the study, a total of 5 different mixtures were obtained. 7, 14, and 28-day non-destructive and 28-day compressive and bending tests of cementitious conductive mortars obtained from five different mixtures were performed. The two-point uniaxial method was used to determine the electrical conductivity properties of the samples. The damping ratio of the samples was obtained by performing dynamic resonance tests. Ultrasound pulse velocity (UPV) and Leeb hardness tests were performed as other non-destructive testing methods. Microstructure analysis at the interfaces of conductive concrete samples was characterized by scanning electron microscopy (SEM), EDS (Energy-Dispersive X-ray Spectroscopy), and X-ray diffraction (XRD). The results showed a logical agreement when comparing their mechanical, physical, and dynamic properties. When SWCNT is used with steel fiber, the conductive mortar samples exhibited good conductivity, while their compressive and bending strengths turned below.

Cite this article as: Dehghanpour, H., Doğan, F., Subaşi, S., & Maraşli, M. (2022). Effects of single-walled carbon nanotubes and steel fiber on recycled ferrochrome filled electrical conductive mortars. *J Sustain Const Mater Technol*, 7(4), 250–265.

1. INTRODUCTION

Cementitious composite materials show great interest in structural elements and large areas such as building facade cladding due to their relatively low cost and easy applicability [1, 2]. Recently, not only the mechanical properties of such applications in modern facade cladding but also their electrical properties have been the subject of research [3]. For some reason, it is preferred to use fine ag- gregate in building facade cladding. The most important reasons are that they are shell elements and the application of the spraying method [4]. Apart from spraying methods, it is preferred to use fine aggregate in ultra-high-perfor- mance concrete (UHPC) shells produced for facade clad- ding [5, 6]. Therefore, the use of conductive additives in a more suitable type and dosage should be investigated to improve the electrical conductivity properties in this building elements mixture.

---

*Corresponding author.
*E-mail address: heydar.dehghanpour@fibrobeton.com.tr

Since 1965 [7], the discovery of electrically conductive cementitious materials, various research have been carried out in this field. Conductive cementitious materials are used in self-sensing [8] materials of buildings, electromagnetic radiation reflectors for electromagnetic interference shielding [9], and resistance materials in self-heating [10] cementitious systems. Electrically conductive cementitious materials have also been proposed as an alternative anti-icing method in snowy weather [11]. Conventional cementitious materials are known to have high electrical resistivity. According to the literature, the resistivity of concrete under room conditions has been reported as 6.54×10^5–11.4×10^5 Ω-cm [12], the resistivity of saturated concrete as 10^6 Ω-cm and the resistivity of thoroughly dried concrete as 10^9 Ω-cm [13, 14]. Using different conductive additives, the researchers even managed to reduce the resistivity values of cementitious materials to just below 100 Ω-cm [12, 13, 15]. Depending on the materials' type, dosage, and conductivity properties, it may vary.

Materials with good conductivity, such as steel fiber [16, 17], carbon fiber [18, 19], erosion wire [20], steel shaving [16], graphite powder [13, 21], carbon nanotube [22], carbon black [20] and graphene [23] can be used to increase the electrical conductivity of cementitious materials. Figure 1 represents the internal structure of electrically conductive concrete [24]. The study used various fibers and nanocarbon black (NCB) materials to provide electrical conductivity. The fibers are randomly placed between aggregates forming a complex network and acting as a bridge for electric current. Cement paste is defined as a matrix element for fibers between aggregates. It has been reported that the electrical conductivity of the fibers increased by combining cement paste with conductive materials in powder form. The NCB fills the intergranular spaces, thus increasing the interface area between the conductive fiber and the matrix. Therefore, it is ensured that the electrical current passes more quickly.

The electrical resistivity of cementitious materials can be measured using a two-point uniaxial, four-probe, or Wenner probe and C1760-12 ASTM [25]. The two-point uniaxial measurement method is the widely used method. In this method, the geometry of the sample can be cylindrical, prismatic, or cube-shaped. The four-probe method is often used to measure the surface resistivity of cylindrical or prismatic specimens. In this method, resistance is measured with four-probe equipment. A voltage difference is applied between the two internal probes, and the electrical current is measured between the two external probes. In the C1760-12 ASTM test method, the electrical resistivity of the hardened saturated cylinder concrete sample is obtained based on the diffusion of chloride ions. This is a two-point-uniaxial test method, but the resistivity may be a little low due to the chloride ion permeability.
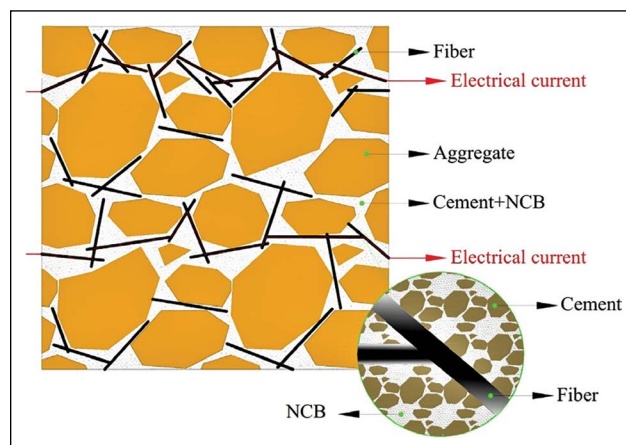

Figure 1. Schematic view of the internal structure of conductive concrete [24].

In the literature, there are many studies on the evaluation of the above-mentioned conductive additives in electrically conductive cementitious materials. However, there are still gaps in the literature on increasing the conductivity of cement and aggregate composition, which are matrix elements in concrete. Also, there are many studies on the evaluation of recycled aggregate and slag materials in concrete [26–28]. The present study investigates the electrical, mechanical, physical, and microstructural properties of electrical conductive mortars containing 100% recycled ferrochrome sand. SWCNT and steel fiber was used as nano and macro-scale conductive additives, respectively. Microstructures of SS-filled, FRC-filled, and FRC-CNT conductive concrete samples were characterized by scanning electron microscopy (SEM), EDS, and X-ray diffraction (XRD). The effects of composite materials on strength were analyzed.

2. MATERIAL AND METHODS

2.1. Used Material
100% silica sand was used as the filling material in the reference mixture, and 100% ferrochrome was used in all other mixtures. The specific gravity of silica sand and ferrochrome sand used were 2.55 and 3.33, respectively. CEM II-42.5 R white cement, preferred in facade cladding, was used as a binder. As a pozzolanic additive material, calcined kaolin was preferred in equal proportions in all mixtures. The chemical composition of Cement, Silica sand, and Calcined kaolin is given in Table 1, and the EDS analysis result of ferrochrome aggregate is shown in Table 2. The particle size ranges of aggregate, cement, and calcined kaolin were compared in Figure 2a, and images of SWCNT and steel fiber used are shown in Figure 2b and Figure 2c, respectively. Stainless steel fiber with a diameter of 80 micrometers and a length of 12 mm was used as the conductive fiber. With a length/diameter ratio of about 1000, SWCNT was added as the nano-sized conductive material. Since the SWCNT used is dispersed in a carboxymethyl cel-

Table 1. Chemical composition of cement, silica sand, and calcined kaolin

Component	Cement (%)	Silica sand (%)	Calcined kaolin (%)
SiO_2	17.460	98.570	59.78
Al_2O_3	3.2700	0.0000	10.23
Fe_2O_3	0.2100	0.1700	0.4400
CaO	63.0400	0.2900	9.9100
MgO	1.6700	0.0000	1.5900
K_2O	0.3400	0.0.16	0.9000
Na_2O	0.3000	0.0000	0.0500
SO_3	3.0200	0.0000	1.2500
P_2O_5	0.0400	0.0100	0.0400
TiO_2	0.0900	0.1200	0.1500
Cr_2O_3	0.0021	0.0137	0.0186
Mn_2O_3	0.0042	0.0029	0.0077
LOI	11.000	0.3900	16.240

Table 2. EDS analysis result of ferrochrome aggregate

Element	Weight %	Weight % Sigma	Atomic %
O	41.85	0.95	49.66
C	12.08	0.49	19.1
Mg	16.7	0.66	13.04
Al	9.39	0.68	6.61
Cr	0	7.14	0
Si	14.29	1.02	9.66
Fe	5.68	1.12	1.93
Total	100		100

lulose-based solution with a ratio of 0.4/1000, more water was used than necessary in the mixtures, according to the preferred 0.3% SWCNT dosage. Polycarboxylate-based superplasticizer was used to ensure adequate workability in all mixtures.

Details of materials used in electrically conductive mortars are given in Table 3. A reference mix is a regular premix mortar consisting of a filler, binder, pozzolanic, water, and plasticizer and is defined as the matrix for other mixtures. In the premix mixture, all dry ingredients are put into the mixer and mixed for 90 seconds; then plasticizer is added with water, remixed for 90 seconds, and placed in molds. In the mixtures containing SWCNT, the water of the solution with SWCNT was taken as the basis instead of mains water. In this case, approximately 88% of water usage will be higher than the reference mixture, and serious adverse effects
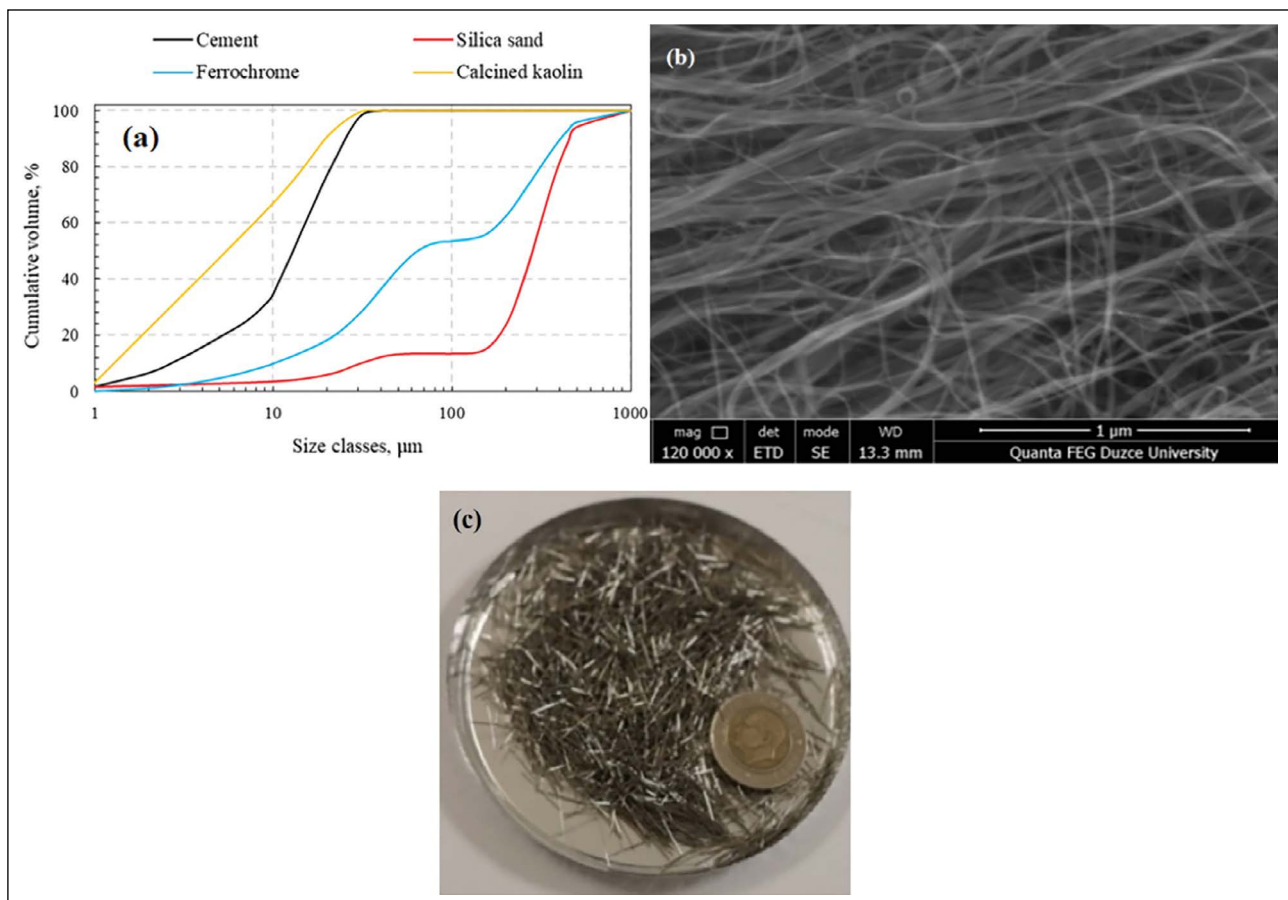

Figure 2. Grain size analysis curves of cement and filling materials **(a)**, SEM image of SWCNT **(b)**, and Steel fiber image **(c)**.

Table 3. Component ratios in electrically conductive mortars

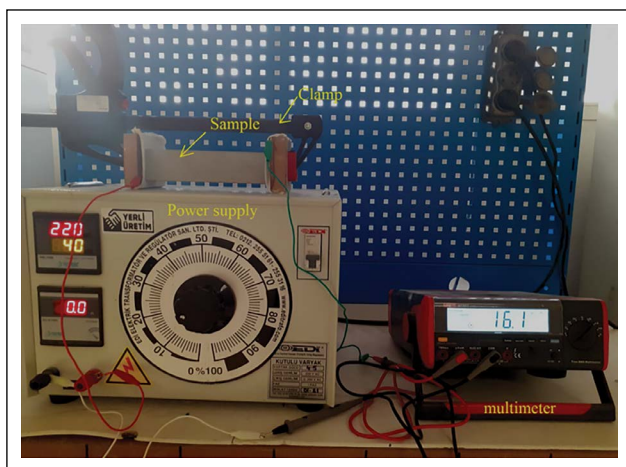| No	Code	Silica sand (g)	Ferrochrome (g)	Cement (g)	Calcined kaolin (CK) (g)	Steel fiber (g)	Su (g)	SWCNT (%)	Superplasticizer (g)
1	SS (Ref)	1350	…	500	50	…	220	…	4
2	FRC	…	1350	500	50	…	220	…	4
3	FRC-SF	…	1245	500	50	105	220	…	4
4	FRC-CNT	…	1350	500	50	…	413	0.3	4
5	FRC-SF-CNT	…	1245	500	50	105	413	0.3	4

Figure 3. Two-point uniaxial electrical conductivity measuring test setup.

are expected on the strength, but since the aim of the study is electrical conductivity, this experiment was considered. After all the components came together in steel fiber mixtures, the fibers were added and mixed with a mixer for one minute when the matrix was ready.

2.2. Test Methods

The electrical conductivity measuring test setup is shown in Figure 3. The measurement of resistances of electrically conductive mortars was carried out by the two-point uniaxial method. This method is also used frequently in the literature [13, 15, 29]. This method applies a potential difference between the two ends of the specimen, and the amount of current realized is measured. The resistance of the specimen is obtained by putting the current value and applied voltage into ohm's law (Eq. 1). The resistivity is calculated from Eq. 2. The electrical conductivity obtained as the inverse of the resistivity is given in Eq. 3.

$$V = IR \qquad (1)$$

$$\rho = R\frac{A}{L} \qquad (2)$$

$$\sigma = \frac{1}{\rho} \qquad (3)$$

The longitudinal resonance frequency analyses of the conductive mortar samples produced from the mixtures obtained within the scope of the study were carried out ac-

cording to the ASTM C215 standard [30]. The experimental setup is given in Figure 4a. According to the resonance test results, firstly, the amplitude-frequency curve (Figure 4b) was drawn for each sample. The damping ratio values were calculated by considering the curve. Many structural problems are solved by determining the natural frequencies at which the structure resonates and the percentage of critical damping of each resonance [31].

In some cases, starting vibration is reduced by changing the active form of the system or shifting a resonant frequency (by stiffening the structure and mass loading) to avoid a frequency coincidence. Another way is to add damping treatments to the structure. Layers of isolation stabilize ground vibration, and installing a vibration absorber can "split" a resonance into two acceptably different frequencies. All these corrections are decided by applying a measured force to the problem structure and measuring and analyzing the response acceleration rate of that force as a function of frequency.

The flexural strengths of the conductive mortar samples were determined by a three-point bending test on three 40 x 40 x 160 mm prismatic samples obtained from each mixture. The parts obtained after the bending test were placed between the apparatus, as in Figure 5, and subjected to the compressive strength test. Bending and compressive strength tests were carried out by the TS EN 196-1 standard [32]. Ultrasonic pulse velocity (UPV) and Leeb hardness tests were performed as non-destructive methods before subjecting them to other tests on identical specimens. UPV tests were performed according to ASTM C597 [33]. The ASTM A956 standard [34] was used to determine the Leeb hardness of the produced samples. In addition, densities were calculated by measuring the dry weight and dimensions of all 28-day samples.

The surface morphologies of the conductive concrete samples were analyzed using HITACHI SU3500 Scanning Electron Microscopy (SEM). After mechanical testing, SEM analyzes were used to observe the porous, rough, and void structure at the sample interface. Elemental analyzes of composite concrete samples were carried out using the Energy-Dispersive X-Ray Spectroscopy (EDS) analysis method. Also, the X-ray Diffraction technique (XRD method) was used to identify the crystalline phases of the materials. XRD analyzes were performed using the RIKAGU device with a scanning range of 10º–70º at a scanning rate of 1º/min.
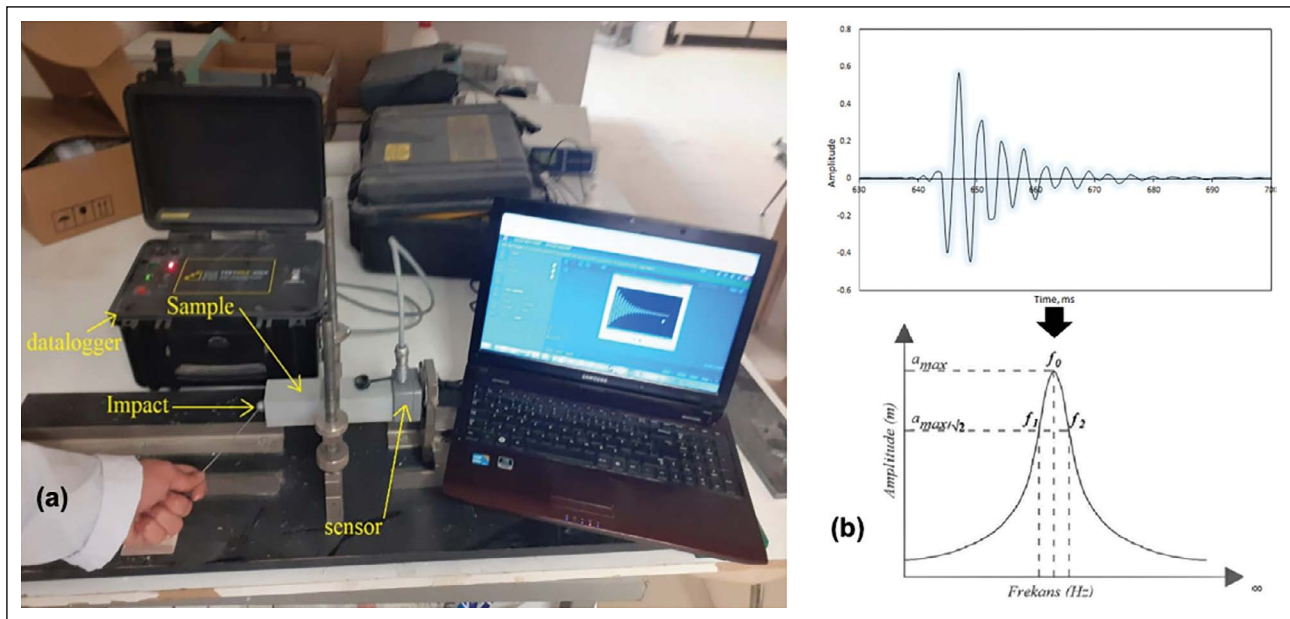
Figure 4. Dynamic resonance test setup **(a)** and schematic view of amplitude-frequency curve.
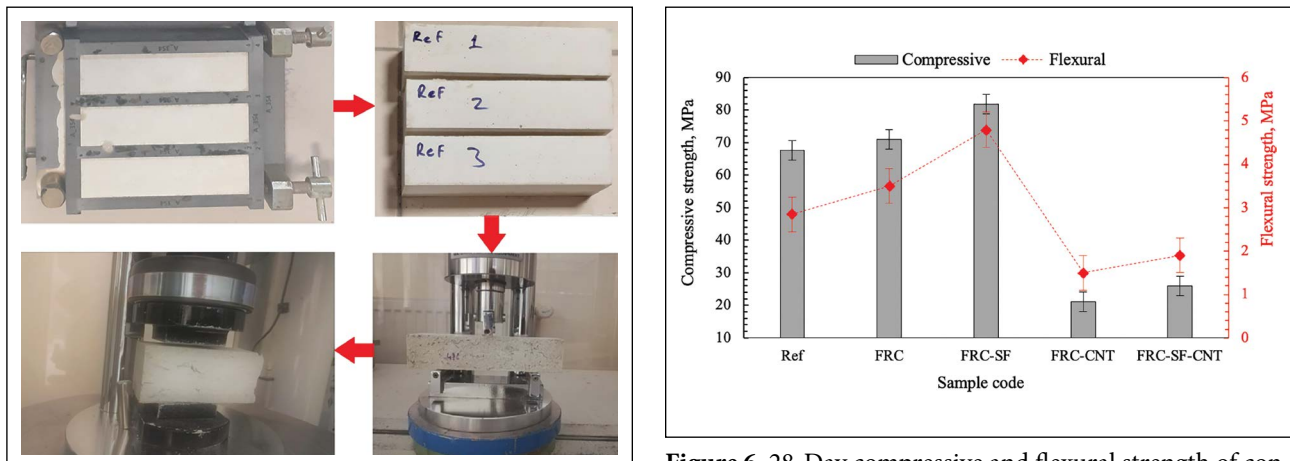

Figure 5. Flexural and compressive strength test setup.

Figure 6. 28-Day compressive and flexural strength of conductive mortar samples.

3. RESULTS AND DISCUSSION

3.1. Mechanical Test Results

As mechanical test methods, 28-day flexural and compressive strength tests of electrically conductive mortar samples were performed, and the most substantial results were compared in Figure 6. The compressive and flexural strength of the ferrochrome (FRC) filled conductive mortar increased by 4.84%, and 22.81%, respectively, compared to the silica sand filled mortar (Ref). This is the significant increase provided by recycled aggregate. Adding five wt.% steel fiber (SF) to the FRC-filled mortar resulted in a 15.26% increase in compressive strength. Also, the strength of this sample was 20.87% higher than that of Ref. The SF contributed 37.14% to the FRC-filled sample's flexural strength, and this sample's flexural strength was 68.42% higher than the

Ref. In the literature, there is information about the positive and negative effects of recycled ferrochrome aggregate on the strength of cementitious materials. In the study of Islam et al. [35], it was reported that the compressive and flexural strength of 100% FRC substituted concrete increased by 12% and 19.9%, respectively, compared to the compressive and flexural strength of concrete filled with natural aggregates. The increase in strength has been explained as the excellent bonding of FRC with cement paste since it has a rough surface [36]. Another reason is that since the FRC has a porous structure, it absorbs the excess water in the concrete and causes a denser matrix formation. At [37], the strength of the obtained concrete decreased with the addition of fine FRC. As a result, the positive or negative effect of FRC on concrete strength is related to factors such
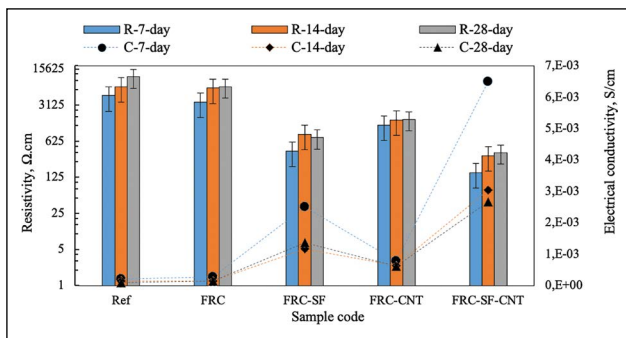
Figure 7. Resistivity and electrical conductivity results of conductive mortar samples.

as FRC's own physical and mechanical properties, granulometry, and water/binder ratio in concrete. According to the graphic, it is observed that carbon nanotube (CNT) has a remarkable negative effect on strength. However, as mentioned above, the high-water content (0.75 of binder) in the dispersed solution is the main reason for this decrease. The reason for using such a high rate of water is that it is aimed to investigate the use of 0.3% pure SWCNT in mixtures. The compressive strength of FRC-CNT decreased by 3.21 and 3.36 times compared to Ref and FRC samples, respectively.

Similarly, flexural strength decreased by 1.9 and 2.33 times, respectively, compared to the same samples. Naqi et al. [38] reported that the compressive strength of cementitious composites containing less than 0.05% MWCNT increased compared to the control sample. On the contrary, they reported that the compressive strength of cementitious composites containing more than 0.05% MWCNT was reduced compared to the control sample. The addition of 5% SF to the FRC-CNT mixture resulted in an increase of 23.41% and 26.67% in compressive and flexural strength, respectively. However, this sample's compressive and flexural strength (FRC-SF-CNT) decreased by 3.14 and 2.53 times, respectively, compared to FRC-SF. Another reason for the decrease in strength may be that the solution containing SWCNT has a high amount of carboxymethyl cellulose (CMC). CMC, which has good water retention, can cause permanent porosity in the matrix after the hydration process is completed when used at high rates in cementitious materials [20]. In a study [39], an increase in the strength of the cementitious composite was observed by using SWCNT dispersed with CMC. The related study used lower rates of CMC (0.3 wt.%) and SWCNT (0.04 wt.%).

3.2. Electrical Properties

7, 14, and 28-day electrical conductivity and resistivity values of the conductive mortar samples are summarized in Figure 7. Depending on the sample age, the resistivity value increased and the electrical conductivity decreased. However, while there was a more significant difference between the seven and 14-day values, the 14 and 28-day

values approached each other. The reason for this is the presence of water in early concrete, which has been proven in previous studies [14, 20] with different voltages on different mixtures. Substitution of FRC sand for silica sand has provided a certain amount of advantage on electrical properties. Considering the 28-day electrical resistivity values, it was observed that the resistivity of the FRC-filled sample decreased by 35.55% compared to Ref. Without the use of conductive fiber, such an improvement in electrical properties is essential in cementitious materials. Because of the improved conductivity as a matrix, it is possible to provide a higher performance current in the presence of conductive fiber. With the addition of 5% SF to the FRC-filled mixture, the electrical resistivity values decreased by about 10-time. With the addition of 0.3 wt.% SWCNT to the FRC-filled mixture, a decrease of more than 4-times in the electrical resistivity values was observed. The electrical resistivity of the FRC-SWCNT-filled mixture decreased approximately four times with the addition of 5 wt.% SF. The resistivity of the same mixture was 19 times lower than the FRC-filled mixture.

The electrical properties of cementitious materials are generally studied for two purposes: durability and physical. It is characterized in terms of chloride penetration in concrete as durability [40]—chlorinated liquids penetrating concrete damage cement products and reinforcement bars. In order to prevent this, the impermeability of the concrete should be reduced. In the study [41], the electrical conductivity of concrete with different ratios of acceptable FRC substitutes instead of natural aggregate was investigated in terms of durability and low chloride ion permeability according to ASTM 1202 [42]. In the literature, there are no studies examining the physical conductivity of FRC filled conductive concretes. The electrical conductivity of natural aggregate-filled concrete varies with the resistivity of the matrix, the type, and ratio of voids, and the type and conductivity level of the conductive additives used. It is known that powder materials generally do not significantly affect concrete's electrical resistivity [20]. For example, El-Dieb et al. [13] found that using carbon powder alone had no significant effect on electrical conductivity. According to the studies, using conductive fiber is essential to increase the conductivity performance in concrete. In the [29] study, the length and ratio of carbon fiber used as conductive fiber were 12 mm and 1%, respectively. Yehia and Tuan [16] obtained optimum conductivity values by using 20% steel shaving and 1.5% steel fiber for an electrically conductive concrete study as a deicing application. Carbon nanotubes (CNT) have been widely used as conductivity-enhancing nanomaterials in cementitious materials [43–45]. Most studies observed the best electrical resistivity values at 1000 Ω.cm when CNT was used alone. However, the functionality of the conductive concrete obtained is divided into various classes accord-

ing to factors such as the purpose of use, CNT ratio, and sample size. It is not sufficient to use CNT alone for the production of heatable, conductive concrete. The best heat performance in heatable conductive concretes is obtained at power consumptions of approximately 500 watts. For this, the most suitable electrical resistivity values are between 200–800 Ω.cm.

Carbon nanotubes' usability in producing new-generation cementitious materials such as self-sensing has been confirmed in different studies [1, 46, 47]. Self-sensing is the ability of a material to respond to different conditions such as temperature, strain, stress, and damage [47]. For example, if a crack occurs in a cementitious material, the resistivity value increases due to the extension of the electric wave propagation way. Since cementitious materials have very high resistivity, it is not easy to measure the resistivity difference in such cases. The presence of conductive materials such as CNT in the cement paste ensures the high sensitivity of the lower resistivity cementitious product. In this study, the alternative mixture that can be used for this purpose may be FRC-CNT. In addition, FRC is a suitable filling material for self-sensing cementitious materials since it is a main part of the direct matrix, and its resistivity is low compared to natural aggregate.

3.3. Non-destructive Test Results

3.3.1. Dynamic Resonance Test Results

The resonant frequency is mainly related to a vibrating beam's dynamic elasticity modulus and density. For this reason, a beam's natural vibration frequency is also used to determine the beam's dynamic modulus of elasticity. In this study, post-resonance test Frequency-Amplitude curves of 7, 14, and 28-day mortars obtained from all mixtures were plotted, and damping ratios were calculated, as shown in Figure 8.

Small peaks at the beginning of the curves are due to ambient noise during testing. Considering the dynamic resonance test results, it is observed that the amplitude number decreases over time; however, the peaks are also narrow. From the amplitude-frequency curves, it can be concluded that the damping ratio increases as the amplitude decreases. In other words, the narrower and higher the curve, the lower the damping; the more comprehensive and lower the curve, the greater the damping [48]. From this information, it can be concluded that the damping ratio decreases with increasing curing time. For example, when the damping ratio of Ref is examined, the damping ratios of 14 and 28 days decreased by 30% and 53%, respectively, compared to 7-day. Considering the damping ratios of FRC and FRC-CNT samples, although CNT had a slight increase effect on the seven and 14-day values, it did not affect the damping ratio of the 28-day sample. When the damping ratios of the FRC and FRC-SF samples were examined, it was observed that SF had an increasing effect of around 40% on
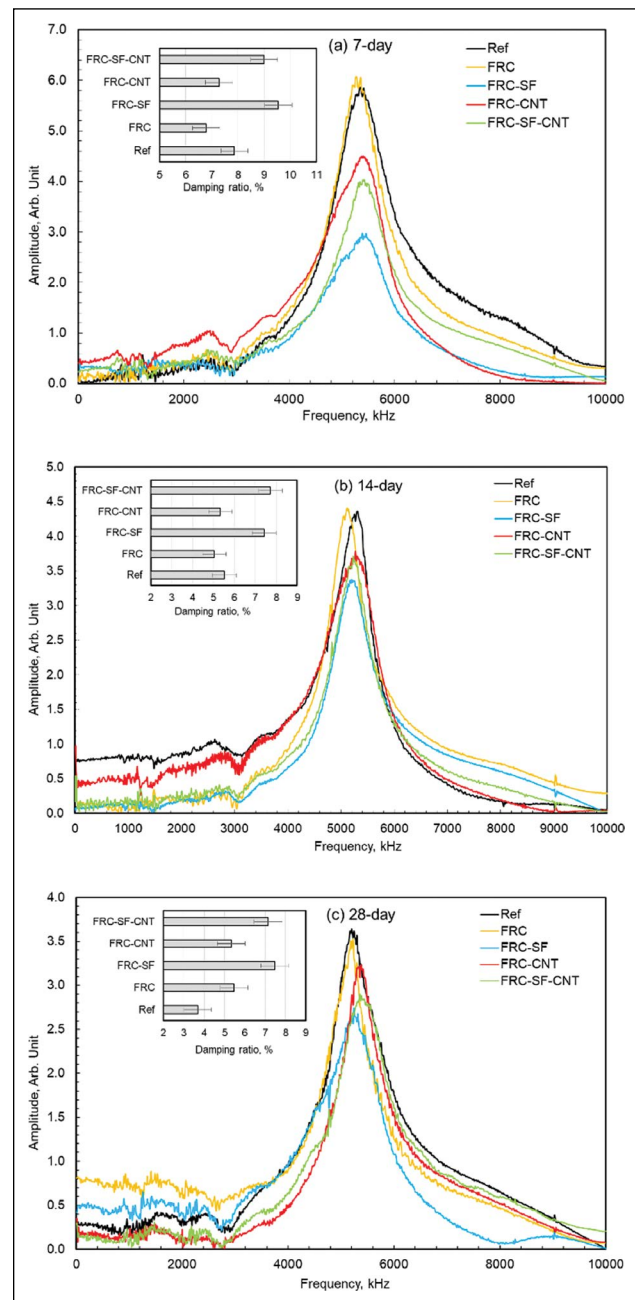

Figure 8. Dynamic resonance test results of conductive mortar samples.

the damping ratio. The damping ratios of the FRC-CNT-SF and FRC-SF samples were almost the same. The positive result obtained with the addition of SF is attributed to the minimization of the defect rate in the mortars [49]. With the increase in energy distribution, a higher capacity damping property emerges. When the damping rates are compared with the mechanical results, it is observed that there is a parallel relationship between them. As in the dynamic results, the maximum values in the mechanical results were obtained for the FRC-SF mixture.
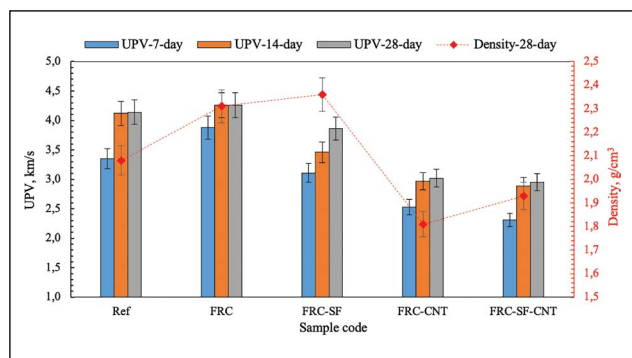
Figure 9. Density and UPV test results of conductive mortar samples.

Figure 10. Leeb hardness test results of conductive mortar samples.

3.3.2. Ultrasonic Pulse Velocity

The ultrasonic pulse velocity results of the samples and the density results are summarized in Figure 9 to observe if there is any correlation between them. When UPV values were compared by age, a more significant incremental variation was observed between 7 and 14-day values, but there was little increase at 28-day values compared to 14-day values. This is due to faster hydration reactions at early ages in cementitious materials. In the early ages, there was more void and water in the matrix, and over time, the hydration products formed due to the hydration reaction filled most of the voids, creating a dense and rigid structure [50]. When the UPV values of the mixtures of FRC and Ref were compared, it was observed that the value of FRC was 2.9% higher than that of Ref. Also, the density value of FRC increased by 11.06% compared to Ref. This is because FRC sand has a denser structure compared to silica sand. As noted in the Material section, the specific gravity values of FRC and silica sand are 3.33 and 2.9 g/cm^3, respectively. With the addition of SF to the FRC mixture, the UPV values decreased by 9.39%. Due to the relatively high dosage of SF (5%), voids occur between the fibers in the mixture. This causes the sound transmission speed to decrease. Although steel fiber had a higher weight compared to concrete, the density of fibrous and fiberless FRC-filled mortars was similar, which is evidence of voids occurring. Due to the extra water used, SWCNT had adverse effects on UPV, density results, and other results. The 28-day UPV and density values of the FRC-CNT mixture decreased by 29.11% and 21.64% compared to the FRC. A similar situation was observed in FRC-CNT-SF. The water/binder ratio significantly affects the density of all cementitious materials [51].

3.3.3. Leeb Hardness Results

The Leeb hardness test, a non-destructive method, provides information about the hardness and estimated strength of construction materials, such as stone and concrete [52, 53]. In the present study, the hardness of prismatic specimens produced from different conductive mortar
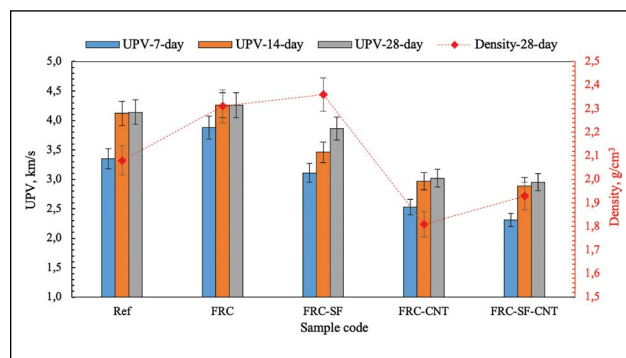
mixtures was measured at different ages and compared in Figure 10. Leeb hardness values increased in all mixtures depending on the sample age. For example, Leeb hardness values of 14 and 28-day Ref samples have increased by 7.8% and 13.8%, respectively, compared to 7-day. Age effect on Leeb hardness was less than others in the FRC mixture. Considering the hardness values of 28-day FRC and silica sand-filled mortars, it was observed that the hardness of FRC-filled mortars was 2% lower. The hardness value of the FRC-filled mortar with SF added was 1.6% higher than the fiberless sample. This is because thin SFs disperse in the mortar and form a network, creating a more rigid surface. SWCNT had a negative effect of 17% on the hardness of the FRC-filled mortar. However, not all of these adverse effects are directly related to SWCNT due to the extra amount of water and CMC used. As indicated in the results above, the amount of extra water used in the mortar caused a high rate of voids and defects in the internal structure. Adding SF to the FRC-CNT mixture increased the hardness value by 13%. When the hardness values were compared with the other results, it was observed that there was a parallel relationship consistent with the compressive, flexural, and density results.

Since there has been no hardness research about FRC filed mortars, it is impossible to compare the obtained hardness values with the literature. However, there are a few Leeb hardness studies on regular concretes, although limited. Song et al. [54] investigated the Leeb hardness of sodium silicate-based concrete and regular C30 concrete and concluded that the average hardness value of standard concrete was 362.4 HL, and that of sodium silicate-based concrete was 405.6 HL. The hardness values of the 28-day specimens produced in this study were measured between 369 and 454 HL. Therefore, the results prove to be compatible when compared to regular concrete. Gomez-Heras et al. [55] stated that the finer the grain size, the higher the Leeb hardness. Also, calcined kaolin improves the surface hardness of concrete [56]. This situation is directly related to filling fine-grained minerals into micro and macropores [57].
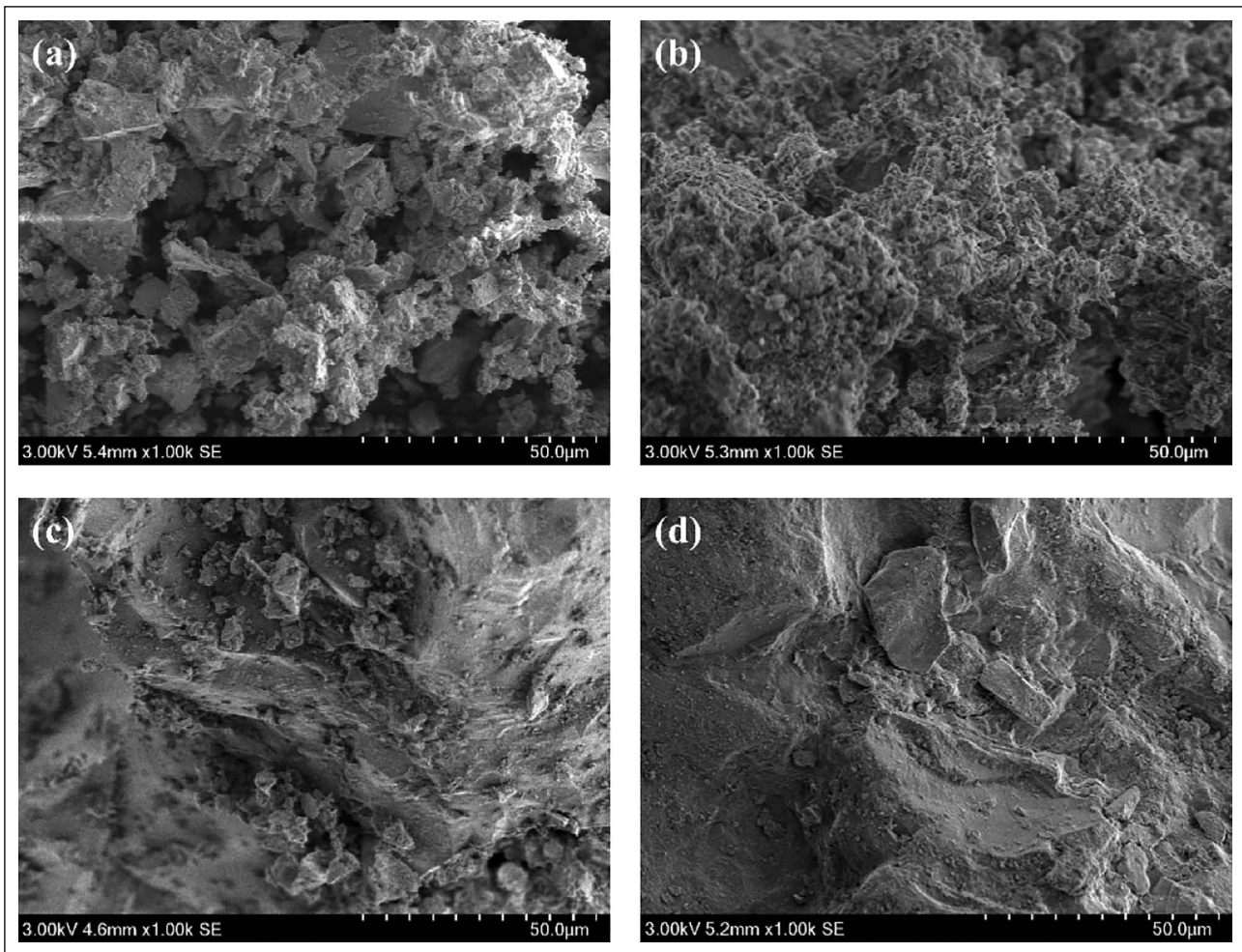
Figure 11. Microstructure images of raw particles; **(a)** cement, **(b)** CK, **(c)** ferrochrome, and **(d)** SS, respectively.

3.4. Microstructure Analysis Results

Figure 11 shows the morphologies of cement, CK, ferrochrome, and SS particles, respectively. The particle sizes were found to be about 5 μm. Ferrochrome and silica sand, used as reinforcement materials, were preferred for their effect on mechanical strength and dense structure formation. Especially the sharp-edged square crystals observed in silica sand reinforcement particles could improve the mechanical behavior of the mixture by strengthening the bond with the cement. It has been known that the micro-voids and micro-cracks formed by the interlocking aggregate particles cause the formation of the porous structure [58]. The effect of particles dispersed in cement on the microstructure was examined. In Figure 12, microstructures of cemented filler samples (SS-filled, FRC-filled, and FRC-CNT) at different magnifications were investigated by SEM analysis. It was observed that the micro-void distributions in the samples were not significant; accordingly, micro-cracks were not formed intensively. In this regard, the micro-voids in the high magnification image of the SS-filled sample (Fig. 12a) was nearly the same in diameter compared to the FRC-filled

sample. It could be stated that the SS-filled sample showed fine microstructure since the microvoids were low compared to the particle size distributions. Fine particle-size silica sand with a large specific surface area increased C-S-H formation in the cement matrix. The increased strength of the compacted samples has been associated with the amount of calcium silicate hydrate (C-S-H) gel in the structure [59].

Aggregate particles were densely combined with the silica sand particles due to intense C-S-H formation. In addition, the silica sand particles in the SS-filled sample contributed to the high gel formation. The silica sand particles improved the morphology of the cementitious matrix and made the matrix denser. Consequently, silica sand particles improved compressive and flexural strength by preventing the formation and development of micro-voids and micro-cracks. Because C-S-H formations were relatively weaker in the FRC-filled cementitious structure microstructure than the SS-filled sample, porosity and roughness increased. The porous and rough structure could be attributed to the air content of the ferrochrome-reinforced cement-based mixture [60].
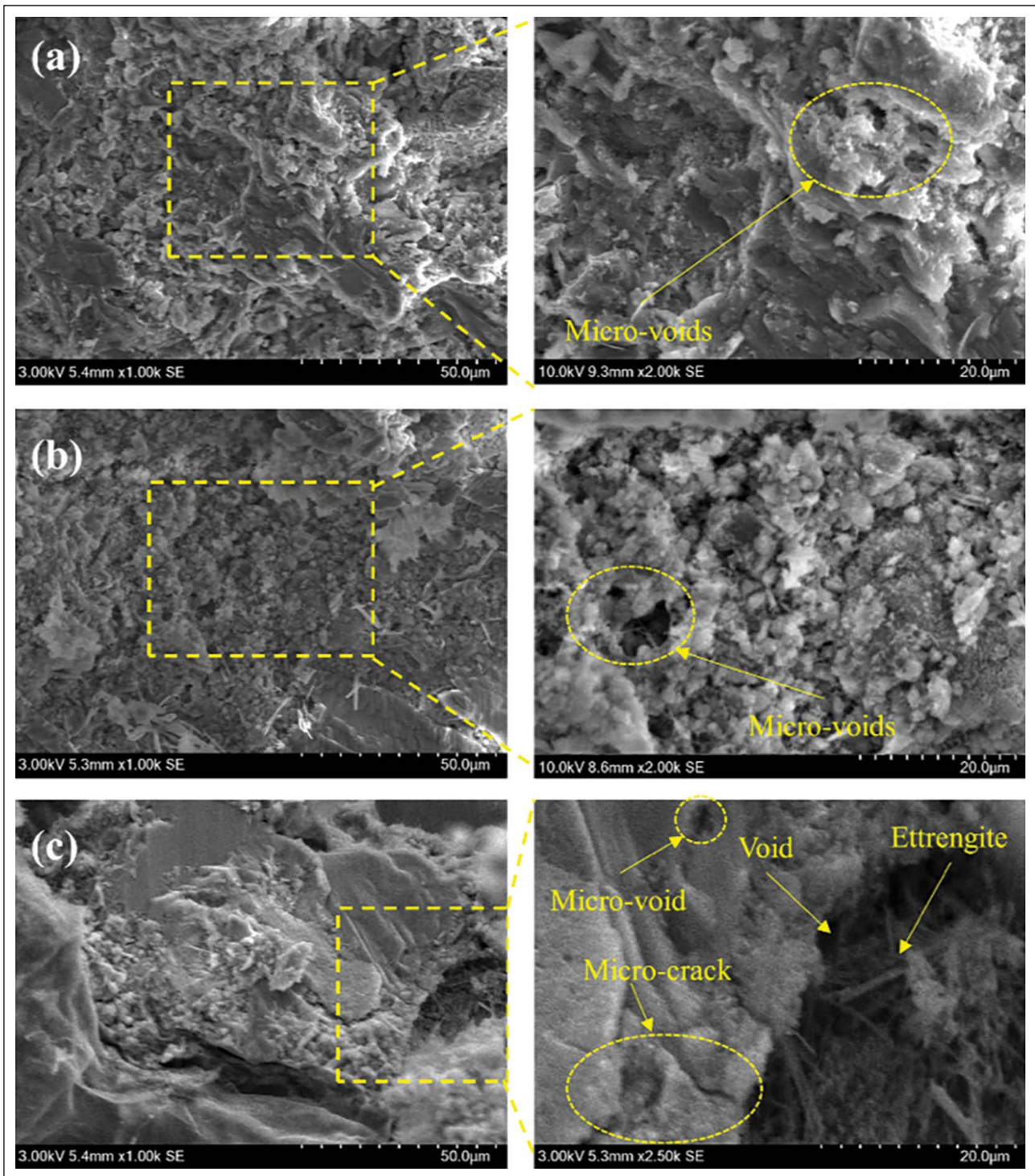
Figure 12. Low and high magnification SEM images of **(a)** SS-filled, **(b)** FRC-filled, and **(c)** FRC-CNT samples, respectively.

The increase in surface roughness compared to the SS-filled sample caused a change in morphology. Nevertheless, the formation of sharp-edged structures seen in the morphology of SS-filled and FRC-filled samples has been attributed to the bonding between aggregate and C-S-H, which increased the material's mechanical strength [61].

The increased compactness of the matrix decreased the tension at the matrix-aggregate interface, preventing the expansion of micro-cracks along with the aggregate. Thus, the reduction in micro-crack contributed to the increase in mortar strength [36]. It could be summarized that SS-filled and FRC-filled samples contained finer particles,

and microstructure deterioration was lower. It has been seen that the FRC-CNT sample was less dense than the other samples. This could be seen as a barrier to strength increase relative to other blends. With the addition of CNT to the mixture, the workability decreased due to the decrease in cement paste. It was observed that CNT particles dispersed in the aggregate could not prevent the formation of voids and cracks. The formation of a larger micro-void structure in FRC-CNT morphology could be attributed to the negative effect of CNT reinforcement on concrete strength. Since C-S-H crystals were collected at the interface, weak bonding in the cement matrix decreased the material's mechanical strength. Moreover, needle-like ettringite crystals observed in cement paste reduced compact structure formation. FRC-CNT sample also pointed out the weakest parameters about density, UPV, and strength tests. It could be said that the addition of CNT particles to the aggregate reduced C-S-H gel formation and made it difficult to form networks in a compact structure.

EDS analysis results of SS-filled, FRC-filled, and FRC-CNT samples are given in Figure 13. O, Si, and Ca elements formed the prominent peaks in the SS-filled sample. The silica in the mixture came from the hydration of the cement, while the gold and palladium came from the gold etching of the samples. The main constituent elements of cementitious products were O, Si, and Ca, and the C/S ratio was related to C-S-H gel formation. Cement-based material products have increased bonding energy by interacting with the matrix interface [62]. The low C/S ratio has been related to high strength [63]. The C/S ratios in the Si-filled, FRC-filled, and FRC-CNT were 1.01, 0.98, and 1.11, respectively. The silica sand added to increase the material durability contains high Si in C-S-H formation; it was observed that the C/S ratio decreased in spectrum-1. Since the increase in C-S-H polymerization increased the degree of interfacial bonding, it supported the formation of the dense and compact structure of the composite material [64]. It has been consistent with the compressive and flexural strength results shown in Figure 6. The absence of micro-cracks in the matrix and aggregate interface region indicated in Figure 12 was attributed to the low shrinkage in the compact structure formed by silica sand.

In spectrum-2, the formation of Cr and Fe element peaks in the FRC-filled sample indicated the presence of ferrochrome particles. Lower C/S level contributed to forming the bonding system between the aggregate/reinforcement particles and confirmed the strength increase noted in Figure 6. Ferrochrome particles containing chromium and iron elements contributed to the mechanical strength increase by collecting C-S-H crystals in the interfacial transition region. Moreover, ferrochrome 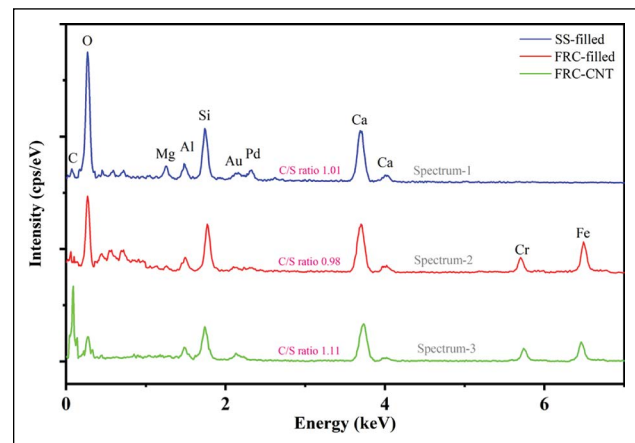with a high percentage of calcium forms high binding in aqueous media with Ca (OH)2 [65]. It could be stated that the intense Ca peak seen in spectrum-2 contributed to the formation of the dense structure of the composite material. The C peak seen in the EDS analysis of the FRC-CNT sample indicated the presence of CNTs in spectrum-3. It could be said that the percentages of Ca and Si were lower due to the high percentage of C that CNTs contain. Thus, it could be concluded that the bond between CNTs and Ca and Si was weak. It could be stated that the decrease in calcium, silicon, chromium, and iron peaks was a weak interaction between CNT and hydration products, and this result could be attributed to the low-density structure indicated in Figure 12. Moreover, CNT allowed the inclusion of more particles compared to chromium and iron elements due to their low density. This explains the increase in the carbon peak and the decrease in the chromium-iron peaks. As a result, as indicated in Figure 7, the conductive CNT particles contributed to the conductivity of the composite material by creating an electric field [66]. When the EDS results are compared with the cemented studies in the literature, the peaks and their grades have been confirmed by the results of several studies [67, 68].

In Figure 14, the phase compositions of SS-filled, FRC-filled, and FRC-CNT samples were shown by XRD models. Origin Pro 2021 software was used to plot the diffraction angles on the X-ray diffraction plot. $CaCO_3$, one of the primary raw materials of cement, contributed to the formation of calcium-containing hydration products such as C-S-H and ettringite [69]. Although it was observed that the primary crystalline peaks in the conductive concrete samples were quartz and calcite, the C-S-H gel also showed characteristic peaks. The silica sand in the SS-filled sample explains the intensity of the quartz main phase. The silica sand content in the cement matrix reduced the ettringite formation and contributed to the compressive strength increase of the composite material. However, it could be
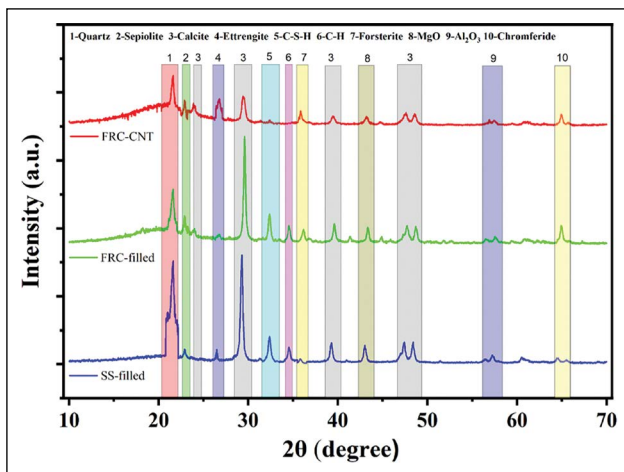

Figure 13. EDS analysis of SS-filled (spectrum-1), FRC-filled (spectrum-2), and FRC-CNT (spectrum-3) samples, respectively.

Figure 14. XRD patterns of SS-filled, FRC-filled, and FRC-CNT.

said that the formation of the ettringite phase in the structure prevented the formation of a porous structure in the composite concrete sample [70]. The reduction of ettringite growth increased the crosslinking within the matrix, thereby forming a compact structure with improved compressive and flexural strengths. The increase in the calcite peak intensity of the SS-filled sample indicated that the hydration process increased, and as a result, it showed that it supported the increase in strength. The increase in C-S-H gel density in the mixture containing silica sand could be explained by the reactivity of the silica sand particles and the high hydration product. Silica sand, which has high hydraulic activity, contributed to the formation of C-S-H gel, which was a product of cement hydration and facilitated the increase of the binding force in the matrix.

In the XRD analysis of ferrochrome-containing samples, forsterite (Mg_2SiO_4) and chromferide (Fe, Cr) mineral peaks were observed separately. Also, it was stated that the analyzed sepiolite mineral was a stable product that intensified the microstructure [71]. In the FRC-filled sample mentioned in Figure 12, the increase in the C-S-H gel content resulting from the hydration reaction was confirmed by the intensity of the calcium silicate hydrate peak observed in the XRD analysis. In addition, the high peak density of portlandite (CH) could be attributed to the conversion of ettringite and portlandite to C-S-H gel, depending on the curing age. In addition, this condition was associated with compressive and flexural strength [72]. The absence of a CNT diffraction peak in the FRC-CNT sample indicated no chemical reaction between the CNT and the cement [73]. Also, it was observed that the CH peak derived from the pozzolanic reactions did not occur. CNTs dispersed in the aggregate cannot be said to contribute to the growth of cement hydrates. It could be argued that CNTs inhibited the hydration process [74]. In addition, the C-H and C-S-H crystals formed because of hydration were not detected in the XRD analysis, which

confirmed this. The ettringite formation confirmed in the SEM microstructural characterization was analyzed in the XRD characterization of the FRC-CNT sample. Although the calcite peak density was associated with the porous structure [75], the bond strength between cement and reinforcement particles did not increase since hydration product formation, such as C-S-H in the FRC-CNT sample, was weak. The decrease in calcite peak intensity could be attributed to the low mechanical strength of the composite concrete of the porous structure formed because of the continuous dissolution of Ca $(OH)_2$.

4. CONCLUSIONS

According to the experimental study, the recycled FRC aggregate positively affected the mechanical properties. The highest compressive and flexural strength results were obtained for the steel fiber-reinforced FRC-filled mixture. SWCNT had an apparent adverse effect on strength. This was primarily related to the CMC used as a dispersing agent. Using FRC sand, the electrical resistivity value was slightly decreased compared to the resistivity of the silica sand-filled reference sample. With the addition of 5% SF, the resistivity value of the FRC-filled mixture decreased significantly. Although SWCNT alone positively affected conductivity properties, it performed best in combination with SF. The presence of SF had an essential role in developing its dynamic properties. Sample age had a positive effect on dynamic properties. An increase of over 53% was observed in the 28-day damping ratio results. When the results obtained with non-destructive test methods are compared with the experimental test results, it has generally proven to be a successful study. A consistent correlation was observed between the UPV and density and strength results.

SEM-EDS and XRD analyses were evaluated together with strength analyses to determine the composite material's performance. The effect of the C/S ratio on compressive and flexural strengths in EDS analysis was discussed. In the SEM analysis, the inclusion of silica sand and ferrochrome particles in the cement mortar contributed to the densification of the composite matrix. XRD results of composite conductive concrete showed that C-S-H gel formation contributed to forming a compact and dense microstructure. It was stated that the C-S-H crystal structures formed because of hydration detected in the XRD analysis affected the increase in strength.

DATA AVAILABILITY STATEMENT

The authors confirm that the data that supports the findings of this study are available within the article. Raw data that support the finding of this study are available from the corresponding author, upon reasonable request.

CONFLICT OF INTEREST

The authors declare that they have no conflict of interest.

FINANCIAL DISCLOSURE

The authors declared that this study has received no financial support.

PEER-REVIEW

Externally peer-reviewed.

REFERENCES

[1] You, I., Yoo, D. Y., Kim, S., Kim, M. J., & Zi, G. (2017). Electrical and self-sensing properties of ultra-high-performance fiber-reinforced concrete with carbon nanotubes. *Sensors* (*Switzerland*), 17(11) Article 2481. [CrossRef]

[2] Li, Z., Ding, S., Yu, X., Han, B., & Ou, J. (2018). Multifunctional cementitious composites modified with nano titanium dioxide: A review. *Composites Part A: Applied Science and Manufacturing*, 111, 115–137. [CrossRef]

[3] Wang, L., & Aslani, F. (2019). A review on material design, performance, and practical application of electrically conductive cementitious composites. *Construction and Building Materials*, 229, Article 116892. [CrossRef]

[4] Ates, A. O., Khoshkholghi, S., Tore, E., Marasli, M., & Ilki, A. (2019). Sprayed glass fiber–reinforced mortar with or without basalt textile reinforcement for jacketing of low-strength concrete prisms. *Journal of Composites for Construction*, 23(2), Article 04019003. [CrossRef]

[5] Marasli, M., Subasi, S., Dehghanpour, H., Ozdal, V., & Kohen, B. (2021). Experimental investigation of pull-out and shear behavior of lifting sockets in precast UHPC panels. *ALKU Journal of Science*, 3(2), 82–93. [CrossRef]

[6] Topbas, A., Tulen, F. Ö., Marasli, M., & Kohen, B. (2019). *A prefabricated GFRC-UHPC shell pedestrian Bridge*. IASS Annual Symposium 2019 – Structural Membranes.

[7] Barnard, E. H., & Tex, H. (1965). *Electrically conductive concrete. Patent No: US3166518A*, 1–2. United States Patent Office.

[8] Howser, R. N., Dhonde, H. B., & Mo, Y. L. (2011). Self-sensing of carbon nanofiber concrete columns subjected to reversed cyclic loading. *Smart Materials and Structures*, 20(8), Article 085031. [CrossRef]

[9] Wen, S., & Chung, D. D. L. (2004). Electromagnetic interference shielding reaching 70 dB in steel fiber cement. *Cement and Concrete Research*, 34(2), 329–332. [CrossRef]

[10] Gomis, J., Galao, O., Gomis, V., Zornoza, E., & Garcés, P. (2015). Self-heating and deicing conductive cement. Experimental study and modeling. *Construction and Building Materials*, 75, 442–449. [CrossRef]

[11] Dehghanpour, H., & Yilmaz, K. (2021). A more sustainable approach for producing less expensive electrically conductive concrete mixtures: Experimental and FE study. *Cold Regions Science and Technology*, 184, Article 103231. [CrossRef]

[12] Wu, J., Liu, J., & Yang, F. (2015). Three-phase composite conductive concrete for pavement deicing. *Construction and Building Materials*, 75, 129–135. [CrossRef]

[13] El-Dieb, A. S., El-Ghareeb, M. A., Abdel-Rahman, M. A. H., & Nasr, E. S. A. (2018). Multifunctional electrically conductive concrete using different fillers. *Journal of Building Engineering*, 15, 61–69. [CrossRef]

[14] Dehghanpour, H., & Yilmaz, K. (2020). Investigation of specimen size, geometry and temperature effects on resistivity of electrically conductive concretes. *Construction and Building Materials*, 250, Article 118864. [CrossRef]

[15] Dehghanpour, H., & Yilmaz, K. (2020). Heat behavior of electrically conductive concretes with and without rebar reinforcement. *Medziagotyra*, 26(4), 471–476. [CrossRef]

[16] Yehia, S. A., & Tuan, C. Y. (2000). Thin conductive concrete overlay for bridge deck deicing and anti-icing. *Transportation Research Record*, 1698(1), 45–53. [CrossRef]

[17] Rao, R., Wang, H., Wang, H., Tuan, C. Y., & Ye, M. (2019). Models for estimating the thermal properties of electric heating concrete containing steel fiber and graphite. *Composites Part B: Engineering*, 164, 116–120. [CrossRef]

[18] Hou, Z., Li, Z., & Wang, J. (2007). Electrical conductivity of the carbon fiber conductive concrete. *Journal Wuhan University of Technology, Materials Science Edition*, 22(2), 346–349. [CrossRef]

[19] Wang, Y. Z., Xu, Y. Z., & Sun, Y. (2012). Experimental study on electrical conductivity of carbon fiber reinforced concrete underwater. *Advanced Materials Research*, 461, 246–249. [CrossRef]

[20] Dehghanpour, H., Yilmaz, K., & Ipek, M. (2019). Evaluation of recycled nano carbon black and waste erosion wires in electrically conductive concretes. *Construction and Building Materials*, 221, 109–121. [CrossRef]

[21] Rao, R., Fu, J., Chan, Y., Tuan, C. Y., & Liu, C. (2018). Steel fiber confined graphite concrete for pavement deicing. *Composites Part B: Engineering*, 155, 187–196. [CrossRef]

[22] Farcas, C., Galao, O., Navarro, R., Zornoza, E., Baeza, F. J., Del Moral, B., Pla, R., & Garcés, P. (2021). Heating and deicing function in conductive concrete and cement paste with the hybrid addition of carbon nanotubes and graphite products. *Smart Materials and Structures*, 30(4), Article 045010. [CrossRef]

[23] Wang, X., Wu, Y., Zhu, P., & Ning, T. (2021). Snow melting performance of graphene composite conductive concrete in severe cold environment. *Materials*, 14(21), Article 6715. [CrossRef]

[24] Dehghanpour, H., Yilmaz, K., Afshari, F., & Ipek, M. (2020). Electrically conductive concrete: A laboratory-based investigation and numerical analysis approach. *Construction and Building Materials*, 260, Article 119948. [CrossRef]

[25] Dehghanpour, H., & Yilmaz, K. (2020). The relationship between resistances measured by two-probe, Wenner probe and C1760-12 ASTM methods in electrically conductive concretes. *SN Applied Sciences*, 2(1), Article 10. [CrossRef]

[26] Dilbas, H. (2022). An investigation on effect of aggregate distribution on physical and mechanical properties of recycled aggregate concrete (RAC). *Journal of Sustainable Construction Materials and Technologies*, 7(2), 108–118. [CrossRef]

[27] Canpolat, O., Uysal, M., Aygörmez, Y., Şahin, F., & Acıkök, F. (2018). Effect of fly ash and ground granulated blast furnace slag on the strength of concrete pavement. *Journal of Sustainable Construction Materials and Technologies*, 3(3), 278–285. [CrossRef]

[28] Dilbas, H. (2021). Application of finite element method on recycled aggregate concrete and reinforced recycled aggregate concrete: A review. *Journal of Sustainable Construction Materials and Technologies*, 6(4), 173–191. [CrossRef]

[29] Sassani, A., Ceylan, H., Kim, S., Gopalakrishnan, K., Arabzadeh, A., & Taylor, P. C. (2017). Influence of mix design variables on engineering properties of carbon fiber-modified electrically conductive concrete. *Construction and Building Materials*, 152, 168–181. [CrossRef]

[30] American Society for Testing and Materials C215. (2019). *Standard test method for fundamental transverse, longitudinal, and torsional resonant frequencies of concrete specimens*. American Society for Testing and Materials.

[31] Trifunac, M. D. (1972). Comparisons between ambient and forced vibration experiments. *Earthquake Engineering & Structural Dynamics*, 1(2), 133–150. [CrossRef]

[32] Turkish Standard EN 196-1. (2005). *Methods of testing cement–Part 1: Determination of strength*. Turkish Standard.

[33] American Society for Testing and Materials C597. (2009). *Standard test method for pulse velocity through concrete*. American Society for Testing and Materials.

[34] American Society for Testing and Materials A956. (2006). *Standard test method for leeb hardness testing of steel products*. American Society for Testing and Materials.

[35] Islam, M. Z., Sohel, K. M. A., Al-Jabri, K., & Al Harthy, A. (2021). Properties of concrete with ferrochrome slag as a fine aggregate at elevated temperatures. *Case Studies in Construction Materials*, 15, e00599. [CrossRef]

[36] Al-Jabri, K., & Shoukry, H. (2018). Influence of nano metakaolin on thermo-physical, mechanical and microstructural properties of high-volume ferrochrome slag mortar. *Construction and Building Materials*, 177, 210–221. [CrossRef]

[37] Dash, M. K., & Patro, S. K. (2018). Performance assessment of ferrochrome slag as partial replacement of fine aggregate in concrete. *European Journal of Environmental and Civil Engineering*, 25(4), 635–654. [CrossRef]

[38] Naqi, A., Abbas, N., Zahra, N., Hussain, A., & Qasim, S. (2018). Effect of multi-walled carbon nanotubes (MWCNTs) on the strength development of cementitious. *Integrative Medicine Research*, 8(1) 1203–1211. [CrossRef]

[39] Uchida, T. (2022). Development of CNT dispersion Al 2 O 3 ceramics. *Ceramics*, 45, 1–4.

[40] Fares, A. I., Sohel, K. M. A., & Al-mamun, A. (2021). Characteristics of ferrochrome slag aggregate and its uses as a green material in concrete – A review. *Construction and Building Materials*, 294, Article 123552. [CrossRef]

[41] Dash, M. K., & Patro, S. K. (2018). Effects of water cooled ferrochrome slag as fine aggregate on the properties of concrete. *Construction and Building Materials*, 177, 457–466. [CrossRef]

[42] American Society for Testing and Materials C1202. (1997). *Standard test method for electrical indication of concrete's ability to resist chloride ion penetration*. American Society for Testing and Materials.

[43] Alessandro, A. D., Tiecco, M., Meoni, A., & Ubertini, F. (2021). Improved strain sensing properties of cement-based sensors through enhanced carbon nanotube dispersion. *Cement and Concrete Composites*, 115, Article 103842. [CrossRef]

[44] Hong, G., Choi, S., Yoo, D., & Oh, T. (2021). Moisture dependence of electrical resistivity in under-percolated cement-based composites with multi-walled carbon nanotubes. *Journal of Materials Research and Technology*, 16, 47–58. [CrossRef]

[45]   Dong, W., Guo, Y., Sun, Z., Tao, Z., & Li, W. (2021). Development of piezoresistive cement-based sensor using recycled waste glass cullets coated with carbon nanotubes. *Journal of Cleaner Production*, 314, Article 127968. [CrossRef]

[46]   Gupta, S., Lin, Y., Lee, H., Buscheck, J., Wu, R., Lynch, J. P., Garg, N., & Loh, K. J. (2021). In situ crack mapping of large-scale self-sensing concrete pavements using electrical resistance tomography. *Cement and Concrete Composites*, 122, Article 104154. [CrossRef]

[47]   Suchorzewski, J., Prieto, M., & Mueller, U. (2020). An experimental study of self-sensing concrete enhanced with multi- wall carbon nanotubes in wedge splitting test and DIC. *Construction and Building Materials, 262*, Article 120871. [CrossRef]

[48]   Tian, J., Fan, C., Zhang, T., & Zhou, Y. (2019). Rock breaking mechanism in percussive drilling with the effect of high-frequency torsional vibration. Energy Sources, Part A: Recovery, *Utilization and Environmental Effects*, 44(1), 2510–2534. [CrossRef]

[49]   Long, W.-J., Wu, Z., Khayat, K. H., Wei, J., Dong, B., Xing, F., & Zhang, J. (2022). Design, dynamic performance and ecological efficiency of fiber-reinforced mortars with different binder systems: Ordinary Portland cement, limestone calcined clay cement and alkali-activated slag. *Journal of Cleaner Production*, 337, Article 130478. [CrossRef]

[50]   Marasli, M., Subasi, S., & Dehghanpour, H. (2022). Development of a maturity method for GFRC shell concretes with different fiber ratios. *European Journal of Environmental and Civil Engineering*, 26(15), Article 2028190. [CrossRef]

[51]   Tassew, S. T., & Lubell, A. S. (2014). Mechanical properties of glass fiber reinforced ceramic concrete. *Construction and Building Materials*, 51, 215–224. [CrossRef]

[52]   Mishra, D. A., & Basu, A. (2013). Estimation of uniaxial compressive strength of rock materials by index tests using regression analysis and fuzzy inference system. *Engineering Geology*, 160, 54–68. [CrossRef]

[53]   Ortega, J. A., Gómez-Heras, M., Perez-López, R., & Wohl, E. (2014). Multiscale structural and lithologic controls in the development of stream potholes on granite bedrock rivers. *Geomorphology*, 204, 588–598. [CrossRef]

[54]   Song, Z., Xue, X., Li, Y., Yang, J., He, Z., Shen, S., … Zhang, N. (2016). Experimental exploration of the waterproofing mechanism of inorganic sodium silicate-based concrete sealers. *Construction and Building Materials*, 104, 276–283. [CrossRef]

[55]   Gomez-Heras, M., Benavente, D., Pla, C., Martinez-Martinez, J., Fort, R., & Brotons, V. (2020). Ultrasonic pulse velocity as a way of improving uniaxial compressive strength estimations from Leeb hardness measurements. *Construction and Building Materials*, 261, Article 119996. [CrossRef]

[56]   Pangdaeng, S., Sata, V., Aguiar, J. B., Pacheco-Torgal, F., Chindaprasirt, J., & Chindaprasirt, P. (2016). Bioactivity enhancement of calcined kaolin geopolymer with CaCl2 treatment. *ScienceAsia*, 42(6), 407–414. [CrossRef]

[57]   García-Del-Cura, M. Á., Benavente, D., Martínez-Martínez, J., & Cueto, N. (2012). Sedimentary structures and physical properties of travertine and carbonate tufa building stone. *Construction and Building Materials*, 28(1), 456–467. [CrossRef]

[58]   Wu, J., Feng, M., Mao, X., Xu, J., Zhang, W., Ni, X., & Han, G. (2018). Particle size distribution of aggregate effects on mechanical and structural properties of cemented rockfill: Experiments and modeling. *Construction and Building Materials*, 193, 295–311. [CrossRef]

[59]   Afzal, M. T., & Khushnood, R. A. (2021). Influence of carbon nano fibers (CNF) on the performance of high strength concrete exposed to elevated temperatures. *Construction and Building Materials*, 268, Article 121108. [CrossRef]

[60]   Dehghanpour, H., Subasi, S., Guntepe, S., Emiroglu, M., & Marasli, M. (2022). Investigation of fracture mechanics, physical and dynamic properties of UHPCs containing PVA, glass and steel fibers. *Construction and Building Materials*, 328, Article 127079. [CrossRef]

[61]   Sun, J., Lin, S., Zhang, G., Sun, Y., Zhang, J., Chen, C., Morsy A. M., & Wang, X. (2021). The effect of graphite and slag on electrical and mechanical properties of electrically conductive cementitious composites. *Construction and Building Materials*, 281, Article 122606. [CrossRef]

[62]   Dehghanpour, H., Doğan, F., & Yılmaz, K. (2022). Development of CNT–CF–Al2O3-CMC gel-based cementitious repair composite. *Journal of Building Engineering*, 45(October 2021), 1–4. [CrossRef]

[63]   Rhee, I., Lee, J. S., Kim, J. H., & Kim, Y. A. (2017). Thermal performance, freeze-and-thaw resistance, and bond strength of cement mortar using rice husk-derived graphene. *Construction and Building Materials*, 146, 350–359. [CrossRef]

[64]   Wang, D., Wang, X., Ashour, A., Qiu, L., & Han, B. (2022). Compressive properties and underlying mechanisms of nickel coated carbon nanotubes modified concrete. *Construction and Building Materials*, 319, Article 126133. [CrossRef]

[65]   Acharya, P. K., & Patro, S. K. (2016). Utilization of ferrochrome wastes such as ferrochrome ash and ferrochrome slag in concrete manufacturing. *Waste Management and Research*, 34(8), 764–774. [CrossRef]

[66]   Lee, S.-J., You, I., Kim, S., Shin, H.-O., & Yoo, D.-Y. (2022). Self-sensing capacity of ultra-high-performance fiber-reinforced concrete containing conductive powders in tension. *Cement and Concrete Composites*, 125, Article 104331. [CrossRef]

[67] Doğan, F., Dehghanpour, H., Subaşi, S., & Maraş-li, M. (2022). Characterization of carbon fiber reinforced conductive mortars filled with recycled ferrochrome slag aggregates. *Journal of Sustainable Construction Materials and Technologies*, 7(3), 145–157. [CrossRef]

[68] Islam, M. Z., Sohel, K. M. A., Al-Jabri, K., & Al Harthy, A. (2021). Properties of concrete with ferrochrome slag as a fine aggregate at elevated temperatures. Case *Studies in Construction Materials*, 15, e00599. [CrossRef]

[69] Akarsh, P. K., Marathe, S., & Bhat, A. K. (2021). Influence of graphene oxide on properties of concrete in the presence of silica fumes and M-sand. *Construction and Building Materials*, 268, Article 121093. [CrossRef]

[70] Pan, D., Yaseen, S. A., Chen, K., Niu, D., Ying Leung, C. K., & Li, Z. (2021). Study of the influence of seawater and sea sand on the mechanical and microstructural properties of concrete. *Journal of Building Engineering*, 42, Article 103006. [CrossRef]

[71] Dash, M. K., Patro, S. K., Acharya, P. K., & Dash, M. (2022). Impact of elevated temperature on strength and micro-structural properties of concrete containing water-cooled ferrochrome slag as fine aggregate. *Construction and Building Materials*, 323, Article 126542. [CrossRef]

[72] Zhang, B., Zhu, H., Shah, K. W., Feng, P., & Dong, Z. (2021). Optimization of mix proportion of alkali-activated slag mortars prepared with seawater and coral sand. *Construction and Building Materials*, 284, Article 122805. [CrossRef]

[73] Li, C. (2021). Chloride permeability and chloride binding capacity of nano-modified concrete. *Journal of Building Engineering*, 41, Article 102419. [CrossRef]

[74] Abedi, M., Fangueiro, R., Camões, A., & Gomes Correia, A. (2020). Evaluation of CNT/GNP's synergic effects on the Mechanical, Microstructural, and durability properties of a cementitious composite by the novel dispersion method. *Construction and Building Materials*, 260, Article 120486. [CrossRef]

[75] Bostanci, L. (2020). Effect of waste glass powder addition on properties of alkali-activated silica fume mortars. *Journal of Building Engineering*, 29, Article 101154. [CrossRef]